Characterization of divalent cation interactions with AASTY nanodiscs

Milena Timcenko,[†] Anton A. A. Autzen,[‡] and Henriette E. Autzen[*,†]

†*Linderstrøm-Lang Centre for Protein Science, Department of Biology, University of Copenhagen, Denmark*

‡*Department of Health Technology, Technical University of Denmark*

E-mail: henriette.autzen@bio.ku.dk

Abstract

Amphiphilic copolymers show great promise in extracting membrane proteins directly from lipid bilayers into 'native nanodiscs'. However, many such copolymers are polyanionic and sensitive to divalent cations, limiting their applicability towards Ca^{2+} or Mg^{2+} dependent proteins. Here, we characterize the Ca^{2+} and Mg^{2+} sensitivity of poly(acrylic acid-co-styrene) (AASTY) copolymers using analytical UV and fluorescent size exclusion chromatography, enabling us to separate signals from nanodiscs, copolymers, and soluble aggregates. Determination of free Ca^{2+} ion concentrations in the presence of copolymer shows that divalent cation tolerance is dependent on not only specific characteristics of a copolymer, but also on its concentration. We see that high ionic strength protects against aggregation facilitated by divalent cations, which is prominent in nanodiscs isolated from excess free copolymer through dialysis. Overall, we conclude that the behavior of amphiphilic copolymers in the presence of divalent cations is more complex than precipitation beyond a specific cation concentration.

Introduction

Membrane proteins are involved in numerous cellular functions and pathways and are important therapeutic targets for a variety of diseases. Characterization of integral membrane proteins by many biochemical and biophysical methods requires their isolation from their native lipid environment; this remains a major bottleneck as initial extraction of membrane proteins from the membrane is typically carried out through solubilization with detergents. However, detergent solubilization can be too harsh for some membrane proteins or complexes as the detergent strips the majority of endogenous lipids and cofactors from the proteins.[1–3] Several approaches for re-lipidating the detergent solubilized membrane protein and reconstituting it into a bilayer mimicking environment have been developed, including membrane scaffold protein (MSP) nanodiscs, Saposin-lipoprotein (Salipro) nanoparticles and peptidiscs.[4–7]

In recent years, amphiphilic copolymers have emerged as an attractive alternative to detergents, as they enable direct solubilization of membrane proteins surrounded by a patch of the surrounding lipid bilayer from the membrane into so-called native nanodiscs.[2,7] Here, the membrane protein remains lipidated and endogenous lipids and cofactors can be preserved around it. Styrene-maleic acid (SMA) copolymers (Figure 1A) were the first to be used for generation of native nanodics and their use remains widespred.[8,9] While the native nanodisc approach shows great promise, there are significant shortcomings with the currently used copolymers; these include their negative charge, and heterogeneity in terms of molecular weight and monomer sequence and effectively limit the applicability of the method to a wider range of protein targets.[10] Alternative copolymers have been published which try to ameliorate these challenges, including poly(diisobutylene-co-maleic acid) (DIBMA),[11] polymethacrylate (PMA),[12] stilbene–maleic anhydride (STMA)[13] and various SMA derivative copolymers.[14–17] The current developments in native nanodiscs have recently been reviewed by e.g. Brown *et al.*[2] and Esmaili *et al.*[9]

Exchanging maleic acid for acrylic acid, we previously showed that poly(acrylic acid-co-

styrene) (AASTY) copolymers (Figure 1B) are effective at solubilizing small, unilameller vesicles (SUVs) as well as extracting a model membrane protein from HEK293 cells.[18] AASTY can be synthesized by reversible addition-fragmentation chain-transfer (RAFT) polymerizations which allows control of copolymer length and dispersity of sizes, compared with other free-radical polymerization methods.[18,19]

Due to the often polyanionic nature of many copolymers including AASTY, one challenge is a sensitivity towards divalent cations such as calcium (Ca^{2+}) and magnesium (Mg^{2+}). This is caused by interactions between the cations and a negatively charged acid subunit. Both Ca^{2+} and Mg^{2+} ions are important for a multitude of cellular processes and are required by many protein for function or integrity.[20,21] Although, the sensitivity of polyanionic copolymers towards divalent cations is well-known, systematic characterization of the effects of divalent cations on amphiphilic copolymers, nanodiscs and the formation of nanodiscs, is limited. The resistance of amphiphilic co-polymers towards Ca^{2+} has typically been characterized through visual inspection, an assessment of turbidity and by dynamic light scattering (DLS).[14,17,22] These are low-resolution techniques, where subtle changes in the solution might not be evident, although they could affect the properties of the copolymer. Furthermore, these techniques record the scattering from an ensamble of particles in the solution and therefore, the signal from nanodiscs and free copolymer remaining in the solution cannot be separated from one another.

An often cited disadvantage of styrene based copolymers is their strong absorption of UV light overlapping with the absorption of proteins at 280 nm, which is commonly used for determination of protein concentration and purity.[11] However, in this study we use this property to our advantage. Using a combination of a photodiode-array (PDA) detector, which records absorption at 190-800 nm, and fluorescent size exclusion chromatography (FSEC), we are able to separate different species not only by size, but also their spectral properties in a straightforward and robust setup. By recording separate signals from fluorescent lipids in nanodiscs and the styrene rich copolymer, we can examine divalent cations effects on

both free copolymer and intact nanodiscs. Along with UV and fluorescence SEC we utilize a colorimetric assay to examine the interactions between the AASTY copolymers and divalent cations. We find that copolymer resistance towards Ca^{2+} and Mg^{2+} ions depends greatly on the copolymer concentration assayed, where higher concentrations are more tolerant. This relates to the binding capacity of the copolymers for the divalent cations, where higher copolymer concentrations result in lower free Ca^{2+} ion concentration compared with a lower copolymer concentration. Binding of divalent cations thereby appear to yield protection against precipitation to some extent. Likewise, including salt in the buffer also yields protection. We further observe that small changes in the AASTY copolymer composition can have a great effect on their behaviour, where higher acrylic acid content results in higher divalent cation tolerance, though the size of the copolymer also play a role. We find that interactions between AASTY copolymers and divalent cations is much more complex than simply defining a concentration threshold for the amount of Ca^{2+} or Mg^{2+} necessary to precipitate the copolymer from solution.

Experimental

Synthesis of AASTY copolymers

The copolymers are the same material as used in Smith *et. Al.*,[18] with the exception of $AASTY_{12.5}$-47. The synthesis of $AASTY_{12.5}$-47 was analogous to the other copolymers. In short, a schlenck flask was charged with azobisisobutyrunitrile (104 mg, 0.634 mmol), the RAFT agent 2-cyano-2-propyl dodecyl trithiocarbonate (1.10 g, 3.17 mmol), and distilled acrylic acid (13.0 g, 190 mmol) and styrene (26.6 g, 232 mmol). The reaction mixture is subjected to 4 freeze-pump-thaw cycles to remove oxygen, and backfilled with nitrogen on a schlenk line. The reaction is heated to 70° C for 9 hours, reaching 95% monomer conversion, resulting in a yellow solid. The solid is dissolved in diethyl ether, and precipitated into hexane, followed by drying in vacuo, resulting in a yellow crisp solid. The dodecyl

trithiocarbonate end group was removed by dissolving copolymer (5 g) in a 1:3 mixture of water:ethanol (40 mL) and 30% H_2O_2 (1.8 mL), and the mixture was incubated at 70°C overnight, resulting in a colorless solution. The product is precipitated by addition to water, and the product is collected by centrifugation. For conversion to a partial sodium salt, the white solid was mixed with water, and NaOH (1 M) is added until the pH is stable at 7.3. The opaque mixture is filtered and lyophilized to yield the partial sodium salt of AASTY.

Determination of free Ca^{2+} concentrations

To measure the concentration of free Ca^{2+} ions in the presence of AASTY or SMA2000 copolymers, copolymers were mixed with buffer for a final composition of 20 mM Hepes/NaOH, pH 7.4, 100 mM KCl and 0 mM, 1 mM, 3 mM or 7 mM $CaCl_2$ and 0.1 % or 1 % copolymer. After 15 minutes incubation, ∼10 µL buffer without copolymer was isolated using a Vivaspin-500 centrifugal concentrator with a 10 MW cutoff (Supp. Figure S1A). In a 96-well plate, 5 µL of this was mixed with 95 µL 0.13 mg/mL o-Cresolphthalein Complexone (oCPC) in 0.1 M CAPS, pH 10. The absorbance at 575 nm was measured on a Tecan Infinite M200 pro microplate reader and quantified based on a standard curve. To ensure that the copolymer had indeed been removed, spectra for select samples were measured using a NanoDrop1000 spectrophotometer.

Formation of empty nanodiscs

Similar to previously described experiments,[18] empty fluorescent nanodiscs were prepared by mixing 1 % copolymer with 1 mM lipids (small unilameller vecicles (SUVs) consisting of 2 % fluorescent Lissamine Rhodamine B phosphatidylethanolamine (LissRhodPE, excitation at 554 nm and emission at 576 nm) and 98 % 1-palmitoyl-2-oleoyl-glycero-3-phosphocholine (POPC)) in 20 mM Hepes/NaOH and 100 mM KCl, or otherwise specified lipid concentration and buffer, in a 100 µL reaction volume. The mixture was incubated for 2 hours at 4^{o}C before ultracentrifugation at 110k g and 4^{o}C for 15 minutes.

To remove free copolymer, the supernatent was dialyzed extensively against a large excess of buffer (three times ∼100 mL per 100 µL sample) using dialysis tubing with a 100 kDa cut-off.

Analysis by FSEC

Prior to analysis by FSEC, the sample was spin filtered through a 0.22 µm filter, to remove any remaining large aggregates. FSEC was run on a Superdex 200 increase column (5/150, Cytiva) attached to a Shimadzu liquid chromatography system equipped with an autosampler (SIL-40), a fluorometer (RF-20A) and PDA detector (SPD-M40). The column was run at a flow rate of 0.2 mL/min in 20 mM Hepes/NaOH pH 7.4 and 100 mM KCl. 2 µL sample was loaded per run for pure copolymer samples (1 % or 0.1 %) and samples directly from solubilization.

To assay effects of KCl and $CaCl_2$ on already formed nanodiscs, the nanodisc samples were diluted 10-fold to change the buffer. In this case the 7.5 µL ND sample was added to 67.5 µL buffer to reach the final specified concentrations. For dialyzed samples 20 µL of the diluted samples was loaded per run, while 10 µL were loaded for ND samples that had not been dialyzed.

SEC data analysis

SEC data was analyzed using NumPy[23] and SciPy.[24] Areas under the curve were calculated using the composite trapezoidal rule through NUMPY.TRAPZ(). To describe the absorption intensity, $I(V)$, as a function of the elution volume, V, a sum of Gaussian functions was fitted using CURVE_FIT from SciPy, using the following equation:

$$I(V) = k + \sum_{n=1}^{m} a_n e^{-\frac{(V-b_n)^2}{2{c_n}^2}}$$

where $m = 3$ for AASTY$_{6.6}$-44, AASTY$_{10}$-47(-ttc), and SMA2000, while $m = 4$ for AASTY$_{8.9}$-45 and AASTY$_{7.4}$-52(-ttc). k is a constant offset to account for a possible background.

All plots were prepared with Matplotlib[25] and schematics of workflows were created with BioRender.com.

Results and Discussion

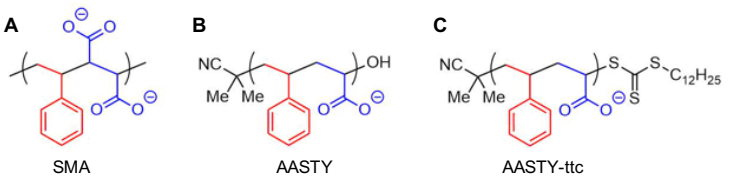

D

Copolymer	Initial AA	Conv. %	AA Cont.	λ	M_n (SEC, kDa)	Đ	Earlier name*
AASTY$_{6.6}$-44	0.40	0.65	0.44	-0.69	6.6	1.19	AASTY-A
AASTY$_{8.9}$-45	0.45	0.96	0.45	-0.72	8.9	1.21	AASTY-B
AASTY$_{7.4}$-52	0.55	0.93	0.52	-0.73	7.4	1.14	AASTY-D
AASTY$_{12.5}$-47	0.45	0.95	0.47	-0,73	12.5	1.12	This work

Figure 1: Overview of copolymers used in this study. Chemical structures of **A)** SMA, **B)** AASTY, and **C** AASTY-ttc with the trithiocarbonate (ttc) end group intact, which absorbs strongly at 310 nm. This end group comes from the RAFT chain transfer agent used during synthesis and is removed in the regular AASTY. **D)** AASTY copolymer characteristics. Abbreviations and symbols used: Acrylic acid, AA; conversion, Conv.; acrylic acid content, AA Cont.; Chemical correlation parameter, λ ($\lambda = 0$ is a perfectly random copolymer, $\lambda = -1$ is perfectly alternating); Number average molecular weight, M_n; dispersity, Đ= M_n/M_w, where M_w is the weight average molecular weight. *The name used in Smith *et al.*[18]

We previously presented and characterized AASTY copolymers in terms of their ability solubilize different lipid compositions and a model mammalian membrane protein.[18] In that study, the AASTY copolymers had masses in the range of 5-8 kDa as this range was previously reported effective for making nanodiscs.[12] In the present work, we added an AASTY copolymer with a molecular weight of 12.5 kDa and acrylic acid content of 47 %, AASTY$_{12.5}$-47, to our library to test the influence of a higher molecular weight on Ca^{2+} sensitivity. To better distinguish different AASTY copolymers as we expand the library in this and future

studies, we here introduce a new naming convention, specifying the acrylic acid content (AA) and number-averaged molecular weight (M_n): AASTY$_{M_n}$-AA (Figure 1D).

RAFT polymerization of the AASTY copolymers result in a terminal Z group consisting of a trithiocarbonate (ttc) moiety that absorbs UV light with a max absorbance at 310 nm. The ttc group was removed for the majority of the copolymers, but included for some samples as a secondary measure of copolymer stoichiometry in disc formation.

Characteristics of the AASTY copolymers used in this study are shown in Figure 1D.

Acrylic acid content governs divalent cation sensitivity

Many proteins depend on Ca^{2+} and Mg^{2+} for their function. Some proteins are sensitive to the specific free Ca^{2+} concentration present, where too high concentrations are inactivating or desensitizing,[26,27] while complete absence of free Ca^{2+} can lead to irreversible inactivation.[26,28] Polyanionic copolymers such as AASTY are chelators of Ca^{2+} through their carboxylate anions. Consequently, the Ca^{2+} concentration that permits native nanodisc formation and stability is not necessarily equivalent to the amount of free Ca^{2+} ions required for a Ca^{2+} dependent protein to function, as the copolymer and protein are competing for Ca^{2+} ions. To shed light on this discrepancy, we used o-Cresolphthalein Complexone (oCPC) in a colorimetric detection of the available Ca^{2+} ions in a solution isolated after exposure to the AASTY copolymers (Figure 2A). Upon chelating divalent cations, oCPC yields a bright purple complex with an absorbance maximum at 575 nm. This allows a comparison of copolymers in terms of divalent cation binding, as the free ions left in solution will interact with oCPC (Figure 2B, Supp. Figure S1A).

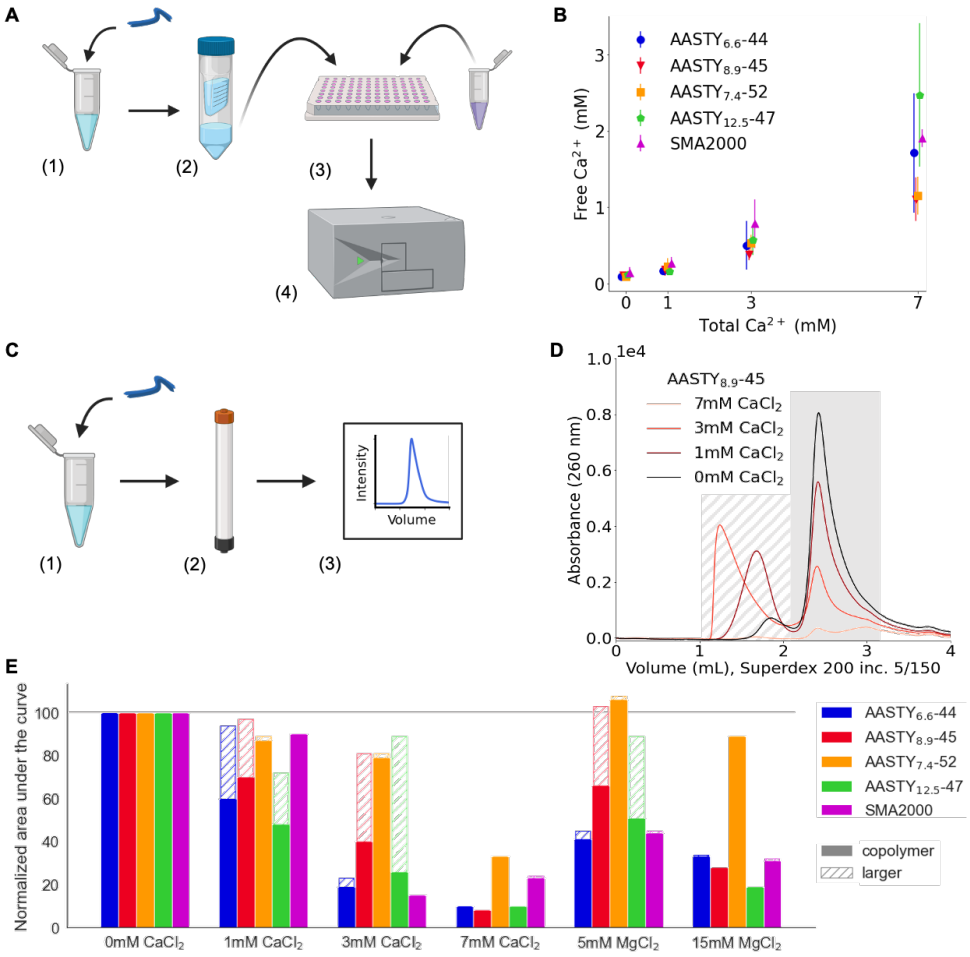

Figure 2: Interaction between free AASTY copolymer and the divalent cations Ca^{2+} and Mg^{2+}. **A)** Free Ca^{2+} concentration was measured using oCPC in the following manner: Solubilized AASTY copolymer was mixed with buffer with or without $CaCl_2$ (1). Next, buffer was isolated from the copolymer using a centrifugal concentrator with a 10 MW cutoff (2), and mixed with oCPC in a 96-well plate (3). Finally, the absorbance at 575 nm was measured using a plate reader (4). **B)** Measurements of free Ca^{2+} concentrations left in solution upon exposure to 1 % copolymer using oCPC. Each measurement was set up in triplicates. Small horizontal shifts have been introduced to separate the data points. Spectra of select samples can be seen in Supp. Figure S1A. **C)** Copolymers were analyzed by SEC by diluting them into a specified buffer (1) followed by loading on a Superdex 200 Increase 5/150 column running in 20 mM HEPES/NaOH, pH 7.4, and 100 mM KCl (2). The copolymer is observed at a wavelength of 260 nm (3, Supp. Figure S2). **D)** SEC of 0.1 % $AASTY_{8.9}$-45 with different concentrations of $CaCl_2$. The running buffer in all instances was without $CaCl_2$. Chromatograms of other AASTY copolymers and with $MgCl_2$ can be found in Supp. Figure S3. The shading indicates the species further quantified in E). **E)** Quantification of the traces from D) and Supp. Figure S3. Areas under the curve were determined separately for the copolymer peak (solid gray in D) and larger species (stripped grey in D) and normalized to the copolymer peak from 0 mM $CaCl_2$ and $MgCl_2$ for each copolymer individually. The grey line indicates 100 %.

The assay with oCPC shows that the divalent cation binding capacity of the four AASTY copolymers included in this work only varies slightly (Figure 2A). Despite a large spread in the data at particularly 7 mM Ca^{2+}, AASTY$_{8.9}$-45 and AASTY$_{7.4}$-52 appear to bind more Ca^{2+} than the larger AASTY$_{12.5}$-47 and SMA2000 that is close in size to the two with an average molecular weight of 7.5 kDa. As such, a higher absolute acrylic acid content is not equal to more binding of Ca^{2+}. AASTY$_{6.6}$-44 has the largest content of styrene and is the most hydrophobic of the AASTY copolymers; its data displays a large spread at both 3 and 7 mM Ca^{2+}, and falls in the middle of the range of the rest of the copolymers.

Across all copolymers and assayed Ca^{2+} concentrations, only 21 % $\pm$ 6 % of the total Ca^{2+} ions remain free in the presence of 1 % copolymer. As could be expected, the degree of Ca^{2+} binding depends on the copolymer concentration, with much higher free Ca^{2+} concentrations in the presence of 0.1 % copolymer as shown for AASTY$_{7.4}$-52 in Supp. Figure S1B.

Turning to the effect of Ca^{2+} and Mg^{2+} on the stability of the AASTY copolymers, i.e. whether the copolymers stay in solution or form insoluble aggregates, we initially looked at pure, solubilized copolymer. Due to the styrene moieties present in both AASTY and SMA, the copolymers absorb light in the UV range. All have a maximum absorbance at 220 nm with decreasing absorbance at longer wavelengths (Supp. Figure S2B), with a local maximum at 260 nm for AASTY. However, possible differences in buffer composition between the sample and running buffer during SEC will also show up at short wavelengths (Supp. Figure S2A), which is why we decided to use the absorbance at 260 nm (A_{260}) to examine the behaviour of the copolymers in the presence of divalent cations.

The tolerance of the AASTY copolymers to Ca^{2+} and Mg^{2+} ions, was determined with SEC, which was performed on copolymer solutions diluted with buffers containing different concentrations of Ca^{2+} or Mg^{2+} (Figure 2C-E). Upon addition of divalent cations, we observed that AASTY$_{6.6}$-44 and AASTY$_{8.9}$-45, and AASTY$_{12.5}$-47 all formed larger species before precipitating, while SMA2000 and AASTY$_{7.4}$-52 precipitated from the solution at specific divalent cation concentrations, with only limited formation of intermediate size ag-

gregates (Figure 2D and Supp. Figure S3). These observations are quantified in Figure 2E for all four AASTY copolymers and SMA2000. While 3 mM $CaCl_2$ was enough to remove much of AASTY$_{6.6}$-44 and SMA2000 from solution, AASTY$_{8.9}$-45 and AASTY$_{12.5}$-47 remaind in solution, but in the form of large soluble species. AASTY$_{7.4}$-52 only significantly aggregated in the presence of 7 mM $CaCl_2$, at which the three other AASTY copolymers also largely precipitated. This experiment highlights the importance of a thorough characterization of the divalent cation tolerance of nanodisc forming copolymers, as it can be overestimated due to soluble aggregates. As evident from Figure 2E, three of the copolymers have a "sweet spot", a divalent ion concentration at which it forms larger species, before it precipitates from the solution.

A similar trend is observed upon addition of Mg^{2+}, though the tolerance is higher for all five copolymers. Here, soluble aggregates are observed for AASTY$_{8.9}$-45 and AASTY$_{12.5}$-47 at 5 mM $MgCl_2$, while only AASTY$_{7.4}$-52 remains significantly in solution at 15 mM $MgCl_2$ (Figure 2E).

In context of the observed Ca^{2+} binding capacities from the oCPC assay (Figure 2B), we see that the copolymers with the lowest apparent binding capacities AASTY$_{6.6}$-44, AASTY$_{12.5}$-47 and SMA2000 are the most sensitive, while one of the copolymers with the highest apparent binding capacity, AASTY$_{7.4}$-52, appears to be the least sensitive to divalent cations. However, while AASTY$_{7.4}$-52 and AASTY$_{8.9}$-45 display equal apparent Ca^{2+} binding capacities, AASTY$_{8.9}$-45 is much more sensitive towards divalent cations. This could be a simple matter of the higher acrylic acid content, and hence charge, of AASTY$_{7.4}$-52 allowing it to withstand a higher level of Ca^{2+} ions before precipitating.

Formation of nanodiscs in the presence of divalent cations

As apparent from the previous section, the copolymers are able to generate larger species in the presence of divalent cations. In some experimental setups, these larger species could be confused for nanodiscs (Figure 2D). Therefore, to be able to monitor the behaviour of

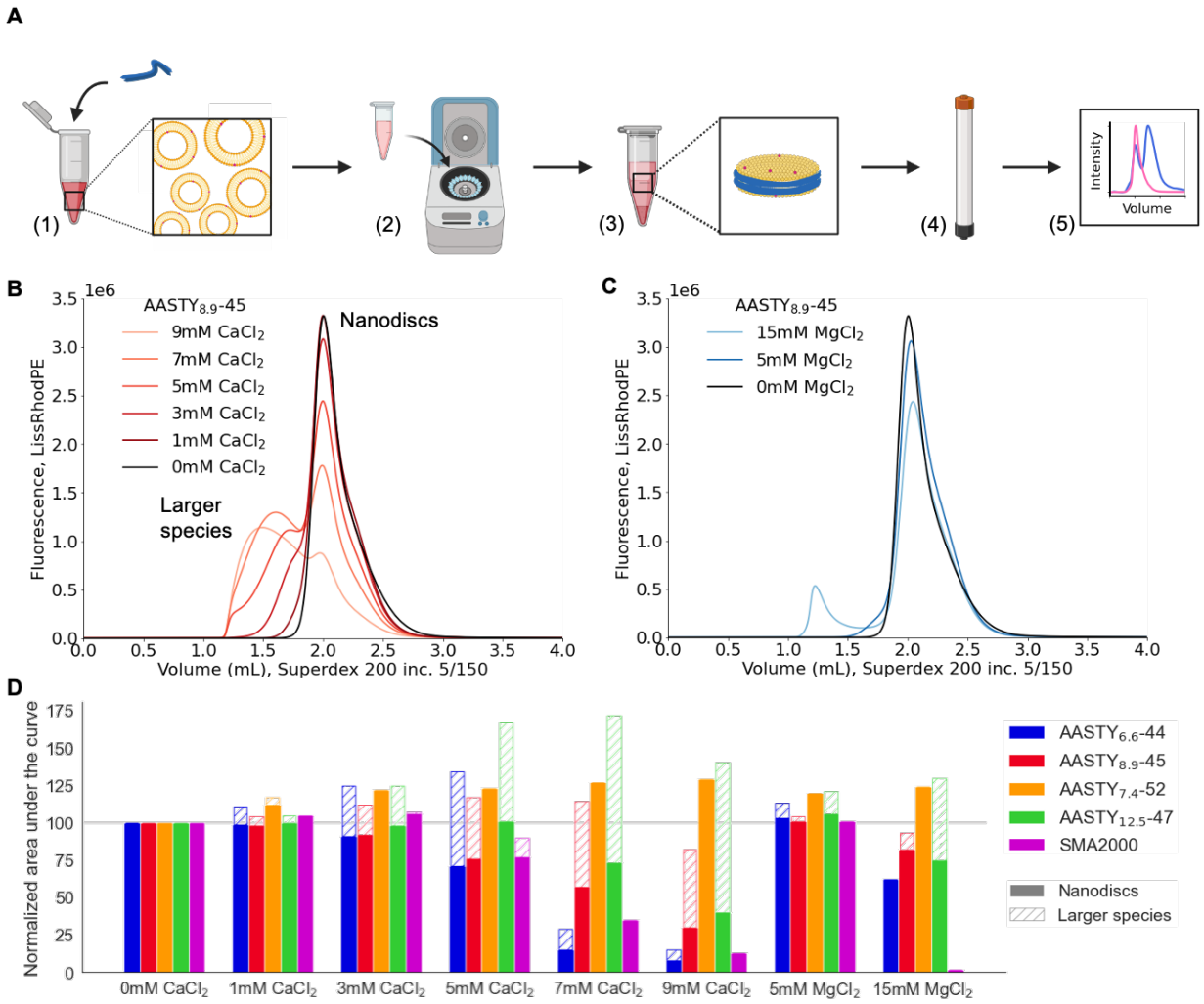

Figure 3: Solubilization of SUVs in the presence of divalent cations. **A)** Fluorescent nanodiscs are produced in the following manner: SUVs of 98 % POPC and 2 % fluorescent LissRhodPE are incubated with copolymer (1) followed by ultracentrifugation (2) to remove insoluble material. The supernatant containing fluorescent nanodiscs and free copolymer (3) is analyzed by FSEC (4,5). **B)** FSEC profiles of nanodiscs generated by solubilizing 1 mM lipids with 1 % AASTY$_{8.9}$-45 in the presence of specified $CaCl_2$ concentrations. **C)** Same as B) with $MgCl_2$. Profiles for the other copolymers can be found in Supp. Figure S5. **D)** Quantification of the area under the curve for the nanodisc peak (at 2 mL) and larger species normalized to the nanodisc peak at 0 mM divalent cations. The nanodisc peak in each trace was determined as the part that falls within the 0 mM trace of that copolymer. The grey line indicates 100 %. A total fluorescence higher than this, could be due to hydrophobic effects increasing the fluorescence from partially aggregated species.

nanodiscs and separate them from any free copolymer present in the solution, we generated fluorescent nanodiscs (Figure 3A), by solubilizing SUVs composed by 98 % POPC and 2 %

of fluorescent LissRhodPE with 1 % copolymer (Figure 3A).

Visualizing the nanodiscs by FSEC, we observe that the five copolymers generate nanodiscs of slightly different sizes (Supp. Fig. S4A). Curiously, the size of produced nanodiscs does not correlate with the size of the copolymer used for solubilization (Supp. Fig. S4B). While AASTY$_{6.6}$-44, AASTY$_{8.9}$-45, and AASTY$_{12.5}$-47 produce discs of very similar sizes, the discs produced by AASTY$_{7.4}$-52 and SMA2000 are somewhat larger. This suggests that nanodisc size is affected by the composition of the copolymer, while the copolymer size itself is inconsequential, at least in the mass range examined here.

Some proteins require a constant presence of calcium and magnesium to retain activity, so adding back the divalent cations after purification might not be sufficient.[26] Therefore, we next sought to characterize which $CaCl_2$ and $MgCl_2$ concentrations would be permissible during nanodisc formation with the four AASTY copolymers and SMA2000 (Figure 3B,C and Supp. Figure S5). As with the pure copolymer, Ca^{2+} ions have a much stronger effect on the stability than Mg^{2+} for all copolymers (Figure 2E and Figure 3D). Likewise, the nanodisc samples behave in a manner similar to the free copolymer as the $CaCl_2$ concentrations increase: The amount of larger, soluble species increases with the $CaCl_2$ concentration, while the portion of well-formed nanodiscs decreases. However, the destabilization is observed at higher Ca^{2+} or Mg^{2+} concentrations.

As with the free copolymer, AASTY$_{7.4}$-52 is least affected by the presence of divalent cations, and while all copolymers tolerate the presence of 3 mM $CaCl_2$ reasonably well, their behaviours start to diverge beyond this point. The AASTY$_{12.5}$-47 nanodisc peak broadens at 5 mM $CaCl_2$ and shifts to larger size at 7 mM and 9 mM $CaCl_2$ (Supp. Figure S5E), but remains in solution. AASTY$_{6.6}$-44 and AASTY$_{8.9}$-45 nanodiscs both form large soluble aggregates before precipitating, though AASTY$_{8.9}$-45 does so at higher $CaCl_2$ concentrations. SMA2000, on the other hand, simply precipitates. Furthermore, only SMA2000 and AASTY$_{6.6}$-44 nanodiscs are not stable in 15 mM $MgCl_2$. These behaviours cannot only be attributed to acrylic acid content, and perhaps the tendency of AASTY$_{12.5}$-47 towards

forming soluble aggregates is caused by its larger size.

Noticeably, all five copolymers appear less sensitive towards Ca^{2+} ions when incorporated into a nanodisc than on their own (compare Figure 3D with Figure 2E). However, it is likely an effect of the higher copolymer concentration present during lipid solubilization (1 %), compared with the SEC experiments with the pure copolymers (0.1 %). This aligns well with our observation that a lower copolymer concentration results in higher free Ca^{2+} concentrations (Supp. Figure S1B), meaning that some Ca^{2+} binding by the copolymer can protect it against precipitation. Taken together these observations show that copolymer resistance towards divalent cations is highly dependent on the assayed copolymer concentration and highlight that a single limiting Ca^{2+} concentration reported for a given copolymer only tells part of the story. The common practice of using turbidity as a measure of divalent cation tolerance can be misleading for describing copolymer lipid nanodisc tolerance of divalent cations. Free copolymer can function as a cushion to the effects of divalent cations on the system, and free copolymer can complex ions and aggregate, without changes in turbidity.

Dialysis removes free copolymer and affects size of discs

In order to examine how the nanodiscs behave, when there is little free copolymer for exchange,[29,30] we removed the free copolymer through dialysis (Figure 4A). Indeed, the copolymer is present in excess in the solubilization experiments described in the previous section, resulting in a large free copolymer peak ("Before dialysis" in Figure 4B,C). During a typical protein purification, this excess copolymer would be removed by e.g. an affinity step. Here, we used a membrane with a 100 kDa cut-off that is just sufficient to retain the nanodiscs. Progression of the dialysis could be monitered through FSEC, with the free copolymer peak becoming smaller after dialysis. It should be noted that dialysis is not feasible for SMA due to its high dispersity.

In addition to removal of excess copolymer, dialysis imposes a shift of the nanodisc peak to slightly lower elution volume for both $AASTY_{8.9}$-45 and $AASTY_{7.4}$-52, with broadening

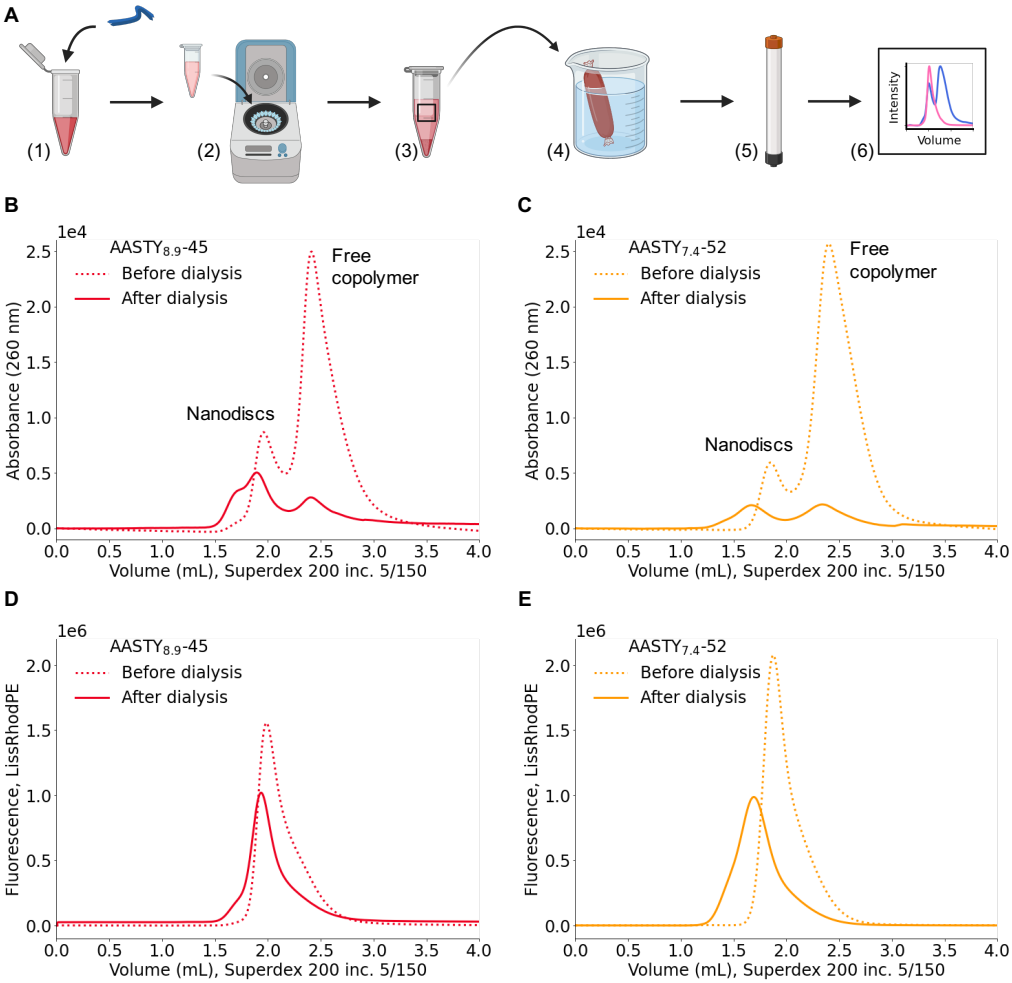

Figure 4: Removal of free copolymer by dialysis. **A)** After generation of fluorescent nanodiscs (1-3, as in Figure 6A), the supernatant is dialysed against a large excess of buffer to remove free copolymer (4), before analysis by FSEC (5,6). Visualization of **B)** AASTY$_{8.9}$-45 and **C)** AASTY$_{7.4}$-52 nanodiscs and free copolymer by absorbance at 260 nm before and and after dialysis. FSEC visualizing the **D)** AASTY$_{8.9}$-45 and **E)** AASTY$_{7.4}$-52 nanodiscs with fluorescent lipids before and after dialysis. The dialysis resulted in 2-3-fold dilution of the sample.

of the AASTY$_{7.4}$-52 nanodisc peak (Figure 4D,E), suggesting that the discs become larger and more disperse in size. This fits with the altered lipid:polymer ratio of these samples, something that has also been observed previously for SMA.[31]

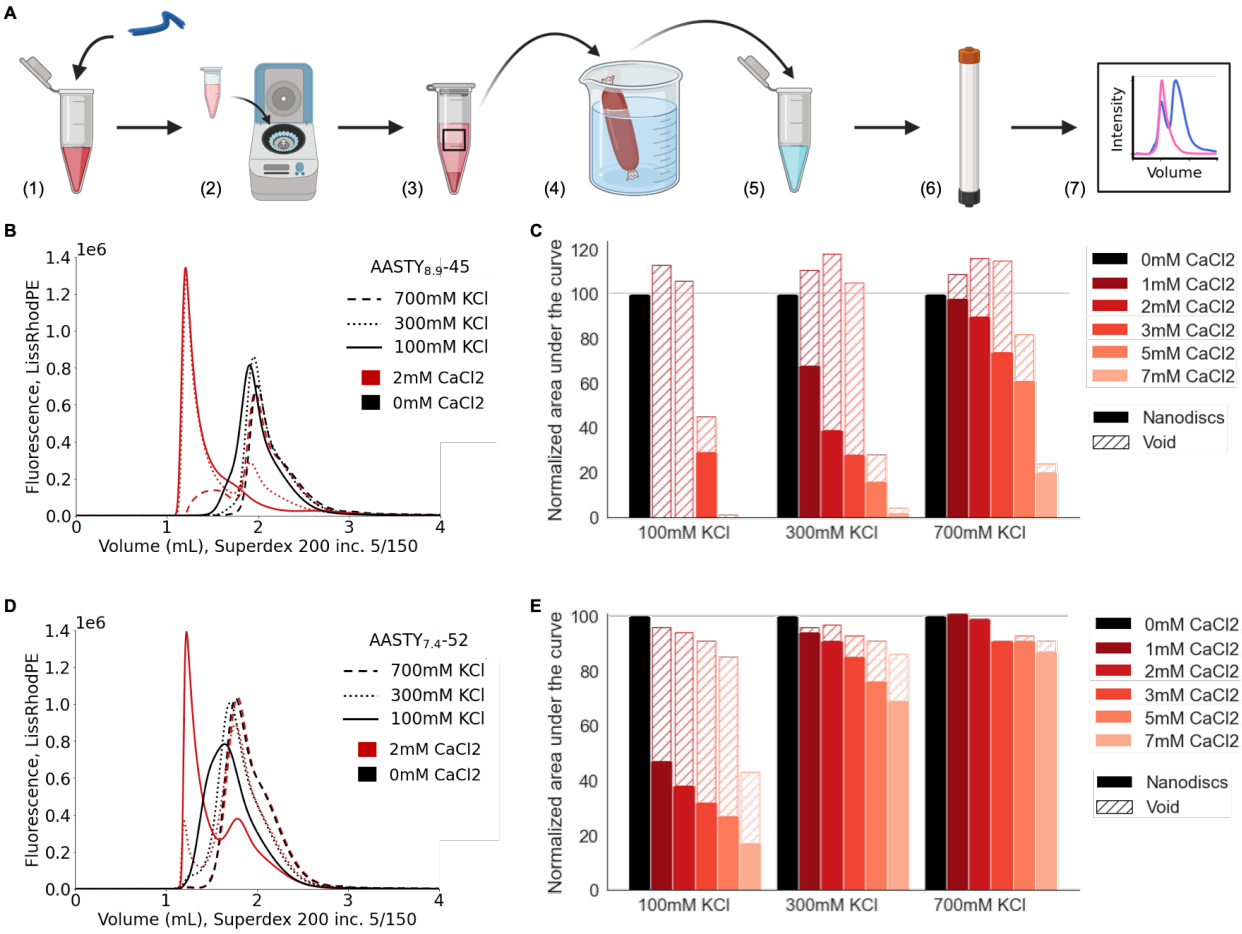

Figure 5: Stability of dialyzed nanodiscs in the presence of Ca^{2+} ions at different ionic strengths. **A)** After removal of free copolymer from a fluorescent nanodisc sample (1-4, as in Figure 4A), the discs were diluted into buffers with varying KCl and $CaCl_2$ concentration (5), before analysis by FSEC (6,7). **B)** Select FSEC traces of fluorescent $AASTY_{8.9}$-45 nanodiscs at different KCl concentrations with or without 2 mM $CaCl_2$, prepared by 10-fold dilution of the dialyzed sample from Figure 4B,D into specified buffer. The running buffer in all instances was 20 mM Hepes/NaOH pH 7.4, 100 mM KCl without $CaCl_2$. Additional $CaCl_2$ concentrations can be found in Supp. Figure S6. **C)** Quantification of the area under the curve for traces from B) and Supp. Figure S6C,E,G divided into void and nanodisc peaks. For each KCl concentration separately, the values were normalized to the 0 mM $CaCl_2$ trace. **D,E)** Same as B,C) but for nanodiscs prepared with $AASTY_{7.4}$-52 (Figure 4C,D). Complete traces for dilutions of the $AASTY_{7.4}$-52 nanodiscs are found in Supp. Figure S7.

Higher salt concentrations stabilize nanodiscs in the absence of free copolymer

To estimate the resistance of the dialyzed nanodiscs against calcium, the samples were diluted 10-fold into buffer with various $CaCl_2$ concentrations and analyzed by FSEC (Figure 5A). A

comparison of the sample prior to dialysis (Supp. Figure S6A and S7A) with the dialyzed sample (Supp. Figure S6C and S7C), reveals that they behave very differently. This is particularly striking for AASTY$_{7.4}$-52, where the sample prior to dialysis appears completely stable at 5 mM $CaCl_2$, while a large part of the dialyzed nanodiscs shift to the void already at 1 mM $CaCl_2$ (compare Supp. Figure S7A and S7C). This substantiates that it is likely calcium binding by AASTY$_{7.4}$-52 that is responsible for its stability. When the free copolymer is removed and the total copolymer concentration is removed, higher free Ca^{2+} concentrations are present as shown in Supp. Figure S1B. Furthermore, this confirms that the apparent high stability of AASTY$_{7.4}$-52 during solubilization in the presence of divalent cations (Figure 3D) is caused by the presence of high amounts of free copolymer, and that the lower tolerance of free copolymer (Figure 2E) is an effect of the lower copolymer concentration assayed. The changes in divalent cation tolerance and binding with changing copolymer concentration is important to take into account when planning experiment with a Ca^{2+} or Mg^{2+} dependent protein.

Observing the very low resistance of the dialyzed nanodiscs against $CaCl_2$ in 100 mM KCl, we speculated that a higher ionic strength might be beneficial if the nanodiscs are simply sticking to each other. This was indeed the case, and higher KCl concentrations both improved the stability of nanodiscs towards Ca^{2+} ions, while also shifting the nanodiscs peak towards longer retention times indicating a slightly smaller size closer to the original nanodisc size (Figure 5B,D). For AASTY$_{7.4}$-52, 300 mM KCl appears enough to recover a lot of the stability of the nanodisc, while 700 mM KCl seems necessary for AASTY$_{8.9}$-45. The behavior is quantified in Figure 5C,E. Possible benefits of high ionic strengths on nanodisc formation has previously been described for SMA[32,33] and DIBMA.[34]

It is worth noting that the nanodisc peak is quite broad for AASTY$_{7.4}$-52 in 100 mM KCl and 0 mM $CaCl_2$ (Figure 5D, solid black). Addition of 2 mM $CaCl_2$, while producing a large void peak, also gives a nanodisc peak, which elutes at slightly lower size and appears sharper (Figure 5D, solid red), suggesting that a higher ionic strength in the buffer is necessary for

$AASTY_{7.4}$-52 nanodiscs to be stable even in the absence of divalent cations.

Evidently, it will be beneficial to screen salt concentrations to fine-tune the sample composition and stability for a specific purpose for a particular transmembrane protein which, like the copolymers, also has a net charge.

Nanodisc size is dynamic and dependent on lipid concentrations

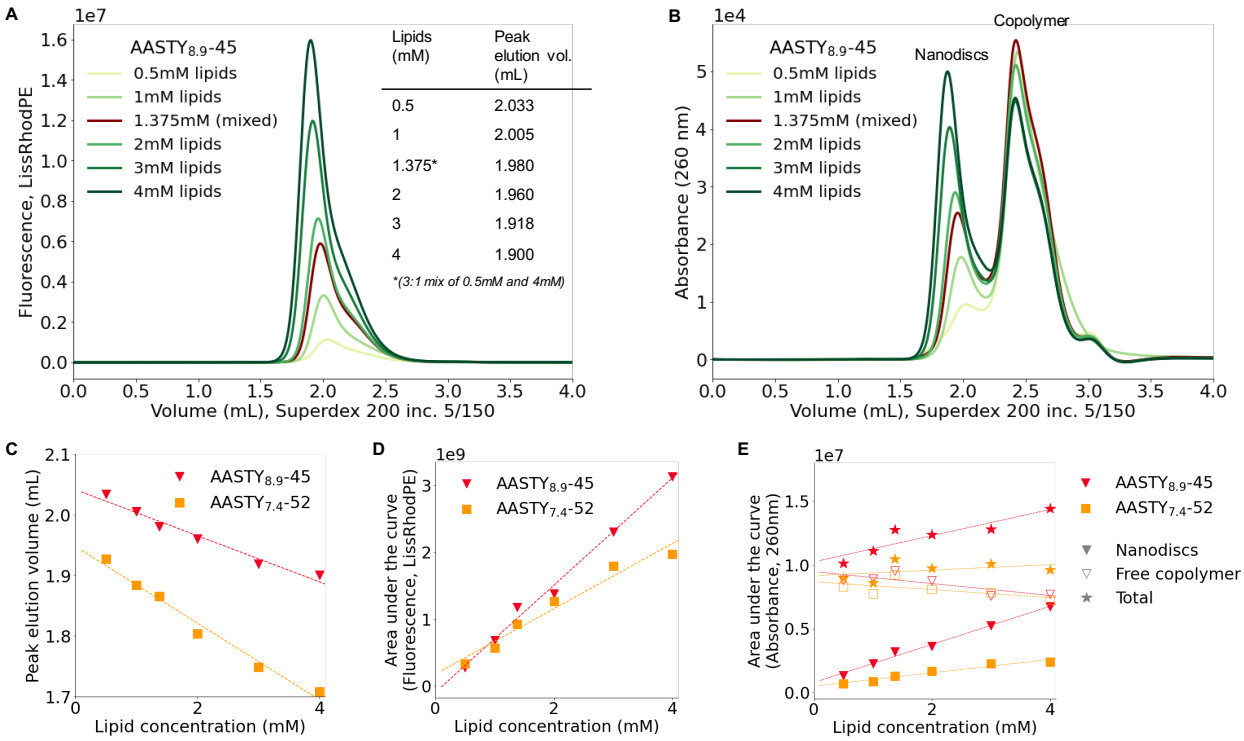

Figure 6: The effect of lipid concentration on nanodiscs size. **A)** FSEC traces of nanodiscs generated by solubilizing different total lipid concentrations (98 % POPC and 2 % LissRhodPE) with 1 % $AASTY_{8.9}$-45. The table insert indicates the elution volume of the peak for different samples. The sample with 1.375 mM lipids (brown trace) was produced by mixing the 0.5 mM and 4 mM samples. **B)** A_{260} for the samples in A). While the nanodisc peak shifts to lower elution volume, the free copolymer peak remains in the same position. **C)** The elution volume of the peak fractions plotted as a function of the lipid concentration. Lower elution volume translates to larger nanodiscs. **D)** Area under the curve from the fluorescent nanodisc signal as a function of the lipid concentration. **E)** Area under the curve from A_{260} for the nanodisc and copolymer peaks separately as well as the total. Plots analogous to A,B for $AASTY_{7.4}$-52 can be found in Supp. Figure S8.

Overall the thermodynamics of nanodisc formation are very complex: Extrinsic factors

such as the ionic strength of the environment and the copolymer concentration affect the apparent size of the nanodiscs (Figure 4B,D and 5). We previously observed that the lipid composition and charge affect AASTY nanodisc formation.[18] Furthermore, the process of nanodisc formation is likely to also be affected by any membrane proteins attempted to incorporate into the nanodiscs. However, intrinsic properties of individual copolymers also play a role (Supp. Figure S4).

To look further into determinants of nanodisc size, we examined the effects of different lipid concentrations on the size of resulting nanodiscs (Figure 6). Here we find that higher lipid concentrations lead to an increase in nanodisc size (Figure 6D). This observation fits well with the increase in nanodisc size seen in the dialyzed nanodisc samples (Figure 4B,D), as the lipid:polymer ratio is increased in both cases. Like we saw during dialysis, nanodiscs are not static, and mixing the largest and smallest nanodiscs leads to nanodiscs of intermediate size, which fall perfectly in line with their resulting lipid concentration (Figure 6A,C). All of these observations are also in line with previous findings of lipid exchange in SMA and DIBMA nanodiscs,[30,35] for which a dependence of nanodisc size on the lipid:polymer ratio has also previously been observed.[11,31]

With increasing lipid concentrations, the area under the curve both for the fluorescent signal from LissRhodPE and the absorbance of the nanodisc peak increase (Figure 6D,E). Curiously, the size of the free copolymer peak only changes little with the amount of lipids solubilized (Figure 6B,E), meaning that the total absorbance of the sample increase though the copolymer concentration is constant. This shows that it is not straightforward to determine the fraction of copolymer that goes into nanodiscs upon solubilization as the spectral properties of free copolymer, and copolymer interacting with lipids appear to be different, likely because of the different chemical environments for styrene. This difference is highlighted when comparing scaled chromatograms from diffrent wavelenghts (Supp. Figure S9A and S10A for AASTY$_{7.4}$-52 and AASTY$_{12.5}$-47). A further complication to quantification is the fact that a copolymer preparation is not perfectly uniform, and each individual copolymer

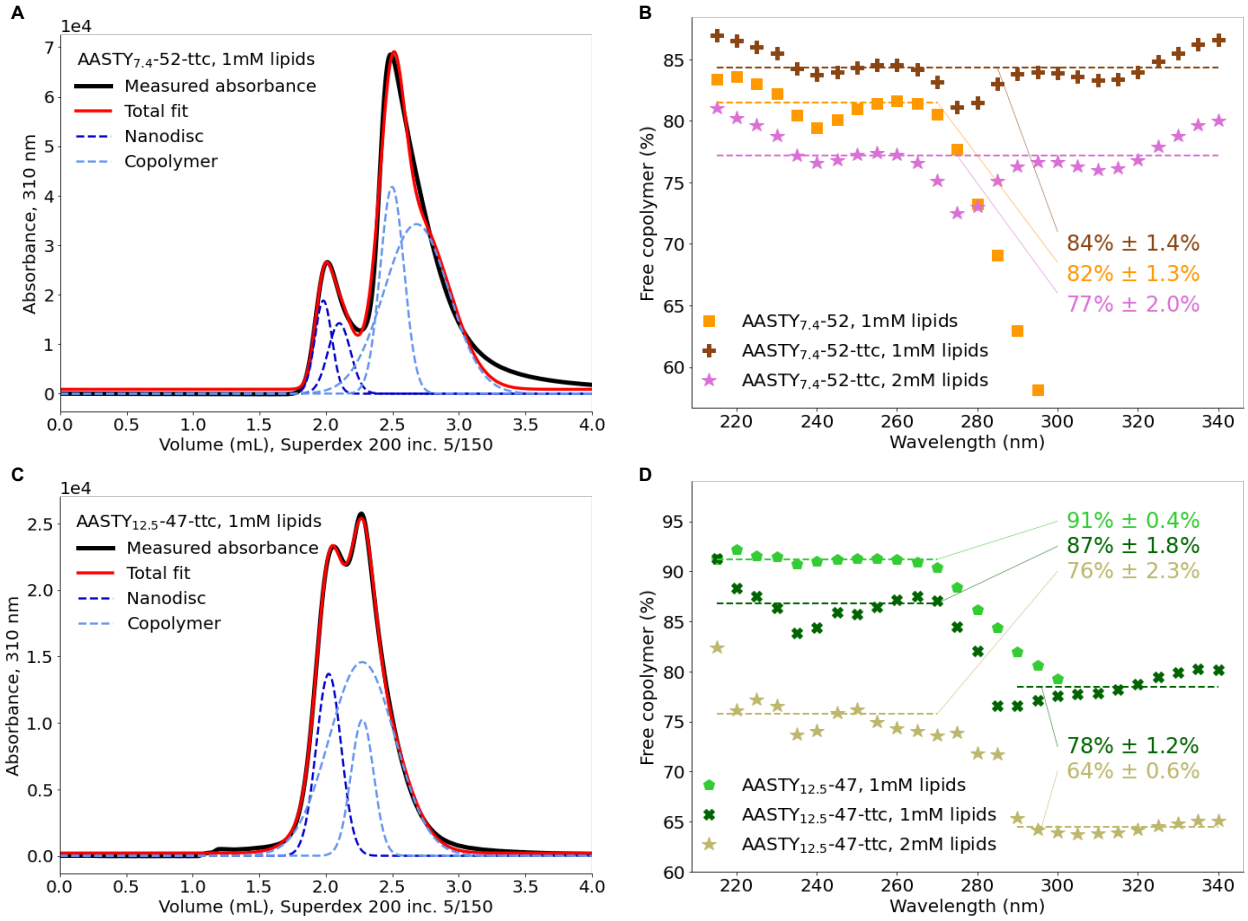

Figure 7: Quantification of free copolymer after solubilization of lipids. **A)** Absorbance at 310 nm for 1 mM lipids (98 % POPC and 2 % LissRhodPE) solubilized with AASTY$_{7.4}$-52-ttc with four Gaussian functions fitted to describe the measured absorbance. Two are attributed to nanodiscs and two to the copolymer. The normalized spectrum of AASTY$_{7.4}$-52-ttc can be found in Supp. Figure S9B,C. **B)** The fraction of free copolymer estimated from the area under the curve of the Gaussian functions describing the copolymer (as shown in panel A) at different wavelengths for AASTY$_{7.4}$-52 and AASTY$_{7.4}$-52-ttc after solubilization of specified lipid concentrations. The average value is indicated on the plot and shown as a dashed line. There is very little signal for AASTY$_{7.4}$-52 at wavelengths longer than 280 nm, and for sample the average is only calculated from wavelengths 215-270 nm. Absorbance profiles at 260 nm for all three samples and the total area under the curve are shown in Supp. Figure S9D,E. **C,D)** Analogous to A,B), but for AASTY$_{12.5}$-47 and AASTY$_{12.5}$-47-ttc. Here, only three Gaussian functions were used to describe the data, where one was attributed to nanodiscs. In D) two different averages were calculated for AASTY$_{12.5}$-47-ttc, as wavelengths dominated by the copolymer and the ttc tag gave very different estimates. Additional data for AASTY$_{12.5}$-47-ttc is shown in Supp. Figure S10.

molecule can have a slightly different absorbance, depending its exact composition.

To circumvent these effect we utilized copolymers with the ttc end group from the RAFT

synthesis (Figure 1C) in solubilization experiments for $AASTY_{7.4}$-52 and $AASTY_{12.5}$-47. ttc absorbs light at 310 nm, and thereby functions as a secondary chromophore to styrene for estimating the distribution of copolymer across differ species. As each copolymer contains exactly one ttc, the signal should be proportional to the number of copolymer molecules.

To quantify the fraction of free copolymers, Gaussian functions were fitted to the chromatogram (Figure 7A,C). This approach was particularly necessary for $AASTY_{12.5}$-47, where the nanodisc peak is a shoulder on the free copolymer (Figure 7C). Calculating the fraction of free copolymer, we observe that the value obtained across different wavelengths is fairly stable for $AASTY_{7.4}$-52 and $AASTY_{7.4}$-52-ttc with 84 % and 82 % of the copolymer population estimated to be free with 1 mM lipids solubilized (Figure 7B). For $AASTY_{12.5}$-47-ttc on the other hand, 87 % is estimated to be free based on wavelengths where styrene absorbs strongly, while 78 % is estimated from those where ttc absorption is dominating (Figure 7D). The overestimation of free copolymers from styrene absorption suggests that styrene absorbs less when engaged in interactions with lipids. However it cannot be completely ruled out that ttc's absorbance is also affected by being lipid associated in nanodiscs.

Looking at the free copolymer fraction as a function of solubilized lipid concentration (Figure 7B,D and Supp. Figure S11) we see that a larger fraction of copolymer is engaged in nanodiscs when more lipids are solubilized, though majority remains free in all tested conditions (Supp. Figure S11).

Finally, the differences in both SEC profiles (Supp. Figures S9C and S10C) and the estimated free copolymer fractions for $AASTY_{7.4}$-52 and $AASTY_{12.5}$-47 with and without the ttc tag (Figure 7B,D) further highlight how very small changes to the chemical structure of a copolymer can have an effect on its performance. It is therefore necessary to benchmark each individual copolymer for the intended purpose.

Conclusions

In this work, we characterize the effects of Ca^{2+} and Mg^{2+} on the stability of AASTY copolymers and nanodiscs using a coupled dye assay and analytical UV and fluorescence SEC. We find that minor differences in the copolymer composition, e.g. its acrylic acid content and molecular mass, have a significant effect on its resistance towards divalent cations. We observe that a higher acrylic acid content conveys a higher apparent tolerance of AASTY for divalent cations. However, this property alone is not sufficient to predict copolymer tolerance as the system is highly affected by the copolymer concentration and excess free copolymer.

Our data shows that the AASTY copolymers tolerate higher concentrations of Mg^{2+} than Ca^{2+}, both on its own and in presence of lipids in nanodiscs. We observe that AASTY copolymers form large, soluble aggregates in addition to precipitating in the presence of divalent cations. For this reason, we utilized the fluorescent lipid LissRhodPE to detect nanodiscs by FSEC and be able to separate the nanodisc signal from any excess free copolymer present in the solution.

Isolating nanodiscs from excess copolymer through dialysis, mimicking e.g. an affinity purification step for a membrane protein, we explored the divalent cation tolerance of nanodiscs in the absence of a large amount free copolymer. We find that the reduced total copolymer concentration reduces the divalent cation tolerance dramatically. However, some the stability of nanodiscs can be rescued by increasing the ionic strength of the buffer.

The spectroscopic properties of the styrene moiety and the ttc end group allowed us to further estimate the fraction of free copolymer from the SEC data. Here, we find that that higher lipid concentrations engage more polymer, while also forming larger nanodiscs. However, majority of the copolymers remain free in all assayed conditions.

At a concentration of 1 %, all four AASTY copolymers as well as SMA2000 bind approximately 80 % of the present Ca^{2+} ions. For AASTY and SMA, which are both negatively charged copolymers, binding of divalent cations appears to play an important role in copolymer tolerance towards these ions: The Ca^{2+} tolerance is dependant on the copolymer

concentration, resulting in preparations with lower copolymer being less stable than those with higher copolymer concentrations. Furthermore, only a fraction of the present Mg^{2+} and Ca^{2+} ions would be accessible to a potential membrane protein of interest, and this concentration would change throughout a protein purification when the copolymer concentration changes. These effects are essential to be aware of when working with Mg^{2+} or Ca^{2+} sensitive membrane protiens in native nanodiscs.

Supporting Information Available

Supporting information contains the following supplementary figures: Absorption spectrum of select oCPC samples and free Ca^{2+} measurement with 0.1 % AASTY$_{7.4}$-52; determination of wavelength to be used for analysis of copolymers by absorption; additional size exclusion chromatograms of pure copolymer and nanodiscs with $CaCl_2$ or $MgCl_2$; analysis of nanodisc size and peak shape for the different copolymers; size exclusion chromatograms of dialyzed nanodiscs of AASTY$_{8.9}$-45 or AASTY$_{7.4}$-52 diluted into buffers with $CaCl_2$ or $MgCl_2$; size exclusion chromatograms of different lipid concentrations solubilized by AASTY$_{8.9}$-45; absorption spectra for quantification of free copolymer fractions in nanodisc samples of AASTY$_{12.5}$-47(-ttc) and AASTY$_{7.4}$-52(-ttc); free copolymer fraction as a function of lipid concentration for various nanodisc preparations; and absorption spectra of copolymer and nanodisc samples from SEC.

Acknowledgement

The authors thank the Novo Nordisk Foundation (NNF20OC0060692) and the Carlsberg Foundation (CF20-0533) for support to equipment and infrastructure. A.A.A.A. was funded by grants NNF18OC0030896 from the Novo Nordisk Foundation and the Stanford Bio-X Program and 0171-00081B from Independent Research Fund Denmark. H.E.A. was funded by grant R265-2017-4015 from the Lundbeck Foundation. Subsets of the figures were created

with BioRender.com.

References

(1) Sun, C.; Benlekbir, S.; Venkatakrishnan, P.; Wang, Y.; Hong, S.; Hosler, J.; Tajkhorshid, E.; Rubinstein, J. L.; Gennis, R. B. Structure of the alternative complex III in a supercomplex with cytochrome oxidase. *Nature* **2018**, *557*, 123–126.

(2) Brown, C. J.; Trieber, C.; Overduin, M. Structural biology of endogenous membrane protein assemblies in native nanodiscs. *Current Opinion in Structural Biology* **2021**, *69*, 70–77.

(3) Marty, M. T.; Hoi, K. K.; Gault, J.; Robinson, C. V. Probing the Lipid Annular Belt by Gas-Phase Dissociation of Membrane Proteins in Nanodiscs. *Angewandte Chemie International Edition* **2016**, *55*, 550–554.

(4) Denisov, I. G.; Sligar, S. G. Nanodiscs for structural and functional studies of membrane proteins. *Nature structural & molecular biology* **2016**, *23*, 481–486.

(5) Frauenfeld, J.; Löving, R.; Armache, J.-P.; Sonnen, A. F.; Guettou, F.; Moberg, P.; Zhu, L.; Jegerschöld, C.; Flayhan, A.; Briggs, J. A., et al. A saposin-lipoprotein nanoparticle system for membrane proteins. *Nature methods* **2016**, *13*, 345–351.

(6) Carlson, M. L.; Young, J. W.; Zhao, Z.; Fabre, L.; Jun, D.; Li, J.; Li, J.; Dhupar, H. S.; Wason, I.; Mills, A. T., et al. The Peptidisc, a simple method for stabilizing membrane proteins in detergent-free solution. *Elife* **2018**, *7*, e34085.

(7) Autzen, H. E.; Julius, D.; Cheng, Y. Membrane mimetic systems in CryoEM: keeping membrane proteins in their native environment. *Current opinion in structural biology* **2019**, *58*, 259–268.

(8) Knowles, T. J.; Finka, R.; Smith, C.; Lin, Y.-P.; Dafforn, T.; Overduin, M. Membrane proteins solubilized intact in lipid containing nanoparticles bounded by styrene maleic acid copolymer. *Journal of the American Chemical Society* **2009**, *131*, 7484–7485.

(9) Esmaili, M.; Eldeeb, M. A.; Moosavi-Movahedi, A. A. Current Developments in Native Nanometric Discoidal Membrane Bilayer Formed by Amphipathic Polymers. *Nanomaterials* **2021**, *11*, 1771.

(10) Dörr, J. M.; Scheidelaar, S.; Koorengevel, M. C.; Dominguez, J. J.; Schäfer, M.; van Walree, C. A.; Killian, J. A. The styrene–maleic acid copolymer: a versatile tool in membrane research. *European Biophysics Journal* **2016**, *45*, 3–21.

(11) Oluwole, A. O.; Danielczak, B.; Meister, A.; Babalola, J. O.; Vargas, C.; Keller, S. Solubilization of membrane proteins into functional lipid-bilayer nanodiscs using a diisobutylene/maleic acid copolymer. *Angewandte Chemie International Edition* **2017**, *56*, 1919–1924.

(12) Yasuhara, K.; Arakida, J.; Ravula, T.; Ramadugu, S. K.; Sahoo, B.; Kikuchi, J.-i.; Ramamoorthy, A. Spontaneous lipid nanodisc fomation by amphiphilic polymethacrylate copolymers. *Journal of the American Chemical Society* **2017**, *139*, 18657–18663.

(13) Esmaili, M.; Brown, C. J.; Shaykhutdinov, R.; Acevedo-Morantes, C.; Wang, Y. L.; Wille, H.; Gandour, R. D.; Turner, S. R.; Overduin, M. Homogeneous nanodiscs of native membranes formed by stilbene–maleic-acid copolymers. *Nanoscale* **2020**, *12*, 16705–16709.

(14) Fiori, M. C.; Jiang, Y.; Altenberg, G. A.; Liang, H. Polymer-encased nanodiscs with improved buffer compatibility. *Scientific reports* **2017**, *7*, 1–10.

(15) Ravula, T.; Ramadugu, S. K.; Di Mauro, G.; Ramamoorthy, A. Bioinspired, Size-Tunable Self-Assembly of Polymer–Lipid Bilayer Nanodiscs. *Angewandte Chemie* **2017**, *129*, 11624–11628.

(16) Ravula, T.; Hardin, N. Z.; Ramadugu, S. K.; Cox, S. J.; Ramamoorthy, A. Formation of pH-Resistant Monodispersed Polymer–Lipid Nanodiscs. *Angewandte Chemie International Edition* **2018**, *57*, 1342–1345.

(17) Hall, S. C.; Tognoloni, C.; Charlton, J.; Bragginton, É. C.; Rothnie, A. J.; Sridhar, P.; Wheatley, M.; Knowles, T. J.; Arnold, T.; Edler, K. J.; Dafforn, T. R. An acid-compatible co-polymer for the solubilization of membranes and proteins into lipid bilayer-containing nanoparticles. *Nanoscale* **2018**, *10*, 10609–10619.

(18) Smith, A. A.; Autzen, H. E.; Faust, B.; Mann, J. L.; Muir, B. W.; Howard, S.; Postma, A.; Spakowitz, A. J.; Cheng, Y.; Appel, E. A. Lipid nanodiscs via ordered copolymers. *Chem* **2020**, *6*, 2782–2795.

(19) Kopf, A. H.; Lijding, O.; Elenbaas, B. O.; Koorengevel, M. C.; van Walree, C. A.; Killian, J. A. Synthesis and Evaluation of a Novel Library of Alternating Amphipathic Copolymers to Solubilize and Study Membrane Proteins. *ChemRxiv* **2021**, This content is a preprint and has not been peer-reviewed.

(20) Clapham, D. E. Calcium signaling. *Cell* **2007**, *131*, 1047–1058.

(21) Jahnen-Dechent, W.; Ketteler, M. Magnesium basics. *Clinical kidney journal* **2012**, *5*, i3–i14.

(22) Danielczak, B.; Meister, A.; Keller, S. Influence of Mg^{2+} and Ca^{2+} on nanodisc formation by diisobutylene/maleic acid (DIBMA) copolymer. *Chemistry and physics of lipids* **2019**, *221*, 30–38.

(23) Harris, C. R.; Millman, K. J.; van der Walt, S. J.; Gommers, R.; Virtanen, P.; Cournapeau, D.; Wieser, E.; Taylor, J.; Berg, S.; Smith, N. J., et al. Array programming with NumPy. *Nature* **2020**, *585*, 357–362.

(24) Virtanen, P.; Gommers, R.; Oliphant, T. E.; Haberland, M.; Reddy, T.; Cournapeau, D.; Burovski, E.; Peterson, P.; Weckesser, W.; Bright, J., et al. SciPy 1.0: fundamental algorithms for scientific computing in Python. *Nature methods* **2020**, *17*, 261–272.

(25) Hunter, J. D. Matplotlib: A 2D graphics environment. *Computing in science & engineering* **2007**, *9*, 90–95.

(26) Møller, J.; Lind, K.; Andersen, J. Enzyme kinetics and substrate stabilization of detergent-solubilized and membraneous (Ca^{2+} + Mg^{2+})-activated ATPase from sarcoplasmic reticulum. Effect of protein-protein interactions. *Journal of Biological Chemistry* **1980**, *255*, 1912–1920.

(27) Prawitt, D.; Monteilh-Zoller, M. K.; Brixel, L.; Spangenberg, C.; Zabel, B.; Fleig, A.; Penner, R. TRPM5 is a transient Ca^{2+}-activated cation channel responding to rapid changes in $[Ca^{2+}]_i$. *Proceedings of the national academy of sciences* **2003**, *100*, 15166–15171.

(28) Champeil, P.; Menguy, T.; Tribet, C.; Popot, J.-L.; le Maire, M. Interaction of amphipols with sarcoplasmic reticulum Ca^{2+}-ATPase. *Journal of Biological Chemistry* **2000**, *275*, 18623–18637.

(29) Schmidt, V.; Sturgis, J. N. Modifying styrene-maleic acid co-polymer for studying lipid nanodiscs. *Biochimica et Biophysica Acta (BBA)-Biomembranes* **2018**, *1860*, 777–783.

(30) Arenas, R. C.; Danielczak, B.; Martel, A.; Porcar, L.; Breyton, C.; Ebel, C.; Keller, S. Fast collisional lipid transfer among polymer-bounded nanodiscs. *Scientific reports* **2017**, *7*, 1–8.

(31) Arenas, R. C.; Klingler, J.; Vargas, C.; Keller, S. Influence of lipid bilayer properties on nanodisc formation mediated by styrene/maleic acid copolymers. *Nanoscale* **2016**, *8*, 15016–15026.

(32) Scheidelaar, S.; Koorengevel, M. C.; Pardo, J. D.; Meeldijk, J. D.; Breukink, E.; Killian, J. A. Molecular model for the solubilization of membranes into nanodisks by styrene maleic acid copolymers. *Biophysical journal* **2015**, *108*, 279–290.

(33) Scheidelaar, S.; Koorengevel, M. C.; van Walree, C. A.; Dominguez, J. J.; Dörr, J. M.; Killian, J. A. Effect of polymer composition and pH on membrane solubilization by styrene-maleic acid copolymers. *Biophysical journal* **2016**, *111*, 1974–1986.

(34) Oluwole, A. O.; Klingler, J.; Danielczak, B.; Babalola, J. O.; Vargas, C.; Pabst, G.; Keller, S. Formation of lipid-bilayer nanodiscs by diisobutylene/maleic acid (DIBMA) copolymer. *Langmuir* **2017**, *33*, 14378–14388.

(35) Danielczak, B.; Keller, S. Collisional lipid exchange among DIBMA-encapsulated nanodiscs (DIBMALPs). *European Polymer Journal* **2018**, *109*, 206–213.

Graphical TOC Entry